ENERGY AND ACCURACY ISSUES IN NUMERICAL SIMULATIONS OF A NON-LINEAR IMPACT MODEL

Stefano Papetti
vipS group, Dept. of Computer Science
University of Verona, Italy
stefano.papetti@univr.it

Federico Avanzini
SMC group, Dept. of Information Engineering
University of Padova, Italy
avanzini@dei.unipd.it

Davide Rocchesso
Dept. of Art and Industrial Design
IUAV University of Venice, Italy
roc@iuav.it

ABSTRACT

A physically-based impact model – already known and exploited in the field of sound synthesis – is studied using both analytical tools and numerical simulations. It is shown that, for some regions of the parameter space, the trajectories of discretized systems may drift from analytically-derived curves. Some methods, based on enforcing numerical energy consistency, are suggested to improve the accuracy and stability of discrete-time systems.

1. INTRODUCTION

Physical models of impacts between objects are ubiquitous in many areas of science and engineering, including robotics, haptics, computer graphics [1], acoustics [2] and sound synthesis [3]. The energetically-consistent and phenomenologically-plausible behavior of contacting bodies is especially crucial in simulations of interactions based on sustained and repeated impacts, as in rolling, scraping, or bouncing.

The classic starting point is the Hertz model of collision between two spheres, which can be extended to include internal viscosity [4]. The restitution force in such model is the sum of a nonlinear elastic term – in the form of a power law of compression – and a dissipative component proportional – via a second power law of compression – to the compression velocity. The exponents of the two power laws, as derived for two colliding balls, are $3/2$ and $1/2$, respectively [5].

The model by Hunt and Crossley [6, 7, 8, 9, 10], which is described in section 2, generalizes the extended Hertz model by considering a variable exponent that accounts for different contact shapes. However, the power laws in the elastic and dissipative term were considered to be equal, thus allowing easier closed-form calculations (in this regard see also Pust and Peterka [11]).

In the context of musical acoustics, Stulov proposed a piano hammer model including the relaxation properties of felt [12]. Such model has exponents α and $\alpha-1$ for the power laws, and the actual value of α can be used to match experimental data.

Other models exist that take plastic deformations into account, thus introducing abrupt direction changes in the force-compression curves at the transition between loading and unloading [13].

2. IMPACT MODEL

The Hunt-Crossley impact model [6] is described by the following non-linear equation

$$f(x,v) = \begin{cases} kx^\alpha + \lambda x^\alpha v = kx^\alpha \cdot (1+\mu v) & , \quad x > 0 \\ 0 & , \quad x \leq 0 \end{cases} \tag{1}$$

where x is the *compression*, $v = \dot{x}$ is the *compression velocity*, $\alpha > 1$ is the *exponent* of a power law and represents the local shape of contact surfaces, k is the *stiffness coefficient*, $0 \leq \lambda \leq k$ is the *damping coefficient*, and $\mu = \lambda/k$ is a mathematically convenient term. The model above represents a non-linear spring of constant k in parallel with a non-linear damper of constant λ. Indeed, kx^α represents the elastic component, while $\lambda x^\alpha v$ represents the dissipation due to internal friction.

Marhefka and Orin [7] made use of the Hunt-Crossley model in order to represent the impact between a lumped point-mass and a rigid wall (representing a comparatively massive surface which does not move during collision), therefore considering the system described by the equation

$$ma(t) = -f(x(t), v(t)), \tag{2}$$

where m is the mass, and a is the mass acceleration. In this very basic case, while the impact interaction lasts, the compression and the compression velocity are respectively equivalent to the displacement and the velocity of the point-mass.

2.1. Properties and analytical results

Thanks to the simple form of (2), the model can be treated analytically and some of its properties can be inferred. Hereafter we consider as initial conditions $x(0) = 0$ and $\dot{x}(0) = v_{\text{in}}$, that is to say that the point-mass hits the rigid wall with velocity v_{in} at time $t = 0$.

2.1.1. Displacement / Compression

It is shown in [7] that from (2) follows

$$x(v) = \left[\frac{m(\alpha+1)}{k\mu^2} \cdot \left(-\mu(v - v_{\text{in}}) + \log \left| \frac{1+\mu v}{1+\mu v_{\text{in}}} \right| \right) \right]^{\frac{1}{\alpha+1}} \tag{3}$$

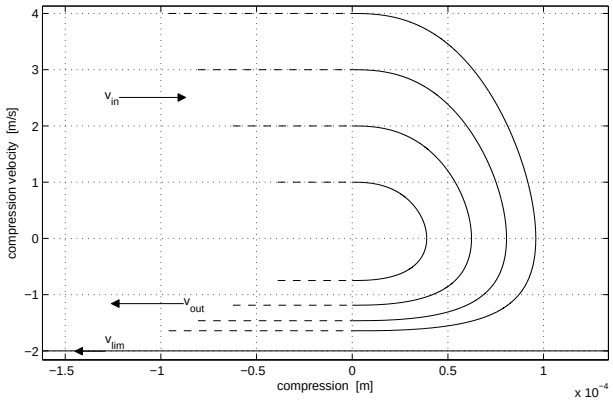

Figure 1: Phase portrait. The values of parameters are: $m = 10^{-2}$ kg, $k = 10^9$ N/m$^\alpha$, $\mu = 0.5$ s/m, $\alpha = 1.5$, $v_{\text{in}} = 1 \ldots 4$ m/s. Solid lines represent the mass trajectory during contact, dashed lines represent free mass motion.

which can be exploited for plotting the phase portrait on the (x, v) plane of figure 1. As figure 1 shows, due to viscous dissipation (represented by λ or μ), the velocity after collision v_{out} is always smaller in magnitude than the corresponding v_{in}. Moreover, for increasing v_{in}, v_{out} converges to the limit value v_{lim}. The line $v = v_{\text{lim}}$ represents the trajectory where the elastic and dissipative terms cancel, and separates two regions of the phase space, each of which is never entered by trajectories started in the other.

It can be noted that (3) allows to infer the *maximum compression* experienced during the impact interaction, which occurs when the compression velocity equals zero. For $v = 0$, equation (3) becomes

$$x_{\max} = x(0) = \left[\frac{m(\alpha+1)}{k\mu^2} \cdot \left(\mu v_{\text{in}} + \log\left|\frac{1}{1+\mu v_{\text{in}}}\right|\right)\right]^{\frac{1}{\alpha+1}}. \tag{4}$$

As remarked by Marhefka and Orin [7], equation (1) together with figure 1 show that the force f becomes sticky (inward) when $v < v_{\text{lim}} \triangleq -1/\mu$. However there is no physical inconsistency in this "stickiness" property, and indeed this never occurs for a trajectory with initial conditions $x(0) = 0$ and $\dot{x}(0) = v_{\text{in}}$.

Finally, by substituting (3) in (2) it is possible to plot the compression-force characteristics during collision, which is shown in figure 2. It can be noted that the dissipative term $\lambda x^\alpha v$ introduces hysteresis around the curve kx^α.

2.1.2. Output velocity

The *restitution coefficient* E is defined as

$$E \triangleq \left|\frac{v_{\text{out}}}{v_{\text{in}}}\right|. \tag{5}$$

In this connection a remark can be made: v_{in} and v_{out} correspond to the roots of the right-hand side of (3), that is the points where $x = 0$. As a result, v_{out} can be defined implicitly from (3) as

$$\mu v_{\text{out}} - \log|1 + \mu v_{\text{out}}| = \mu v_{\text{in}} - \log|1 + \mu v_{\text{in}}| \tag{6}$$

where v_{out} is defined as a function of (μ, v_{in}). This implies that μv_{out} is a function of μv_{in} only, and therefore E is also a function

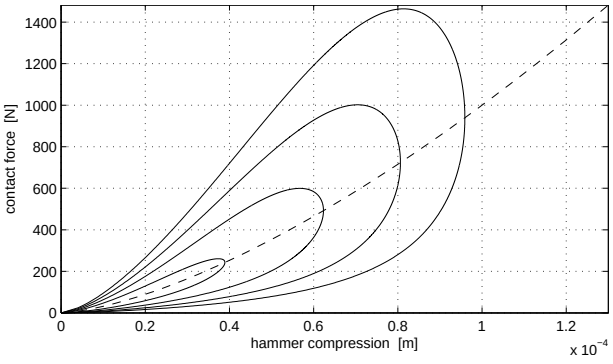

Figure 2: Compression-force characteristics. Solid lines represent the case when dissipation is taken into account (the values of parameters are the same as in figure 1). The dashed line represents the case when $\lambda = 0$, that is no dissipation is considered.

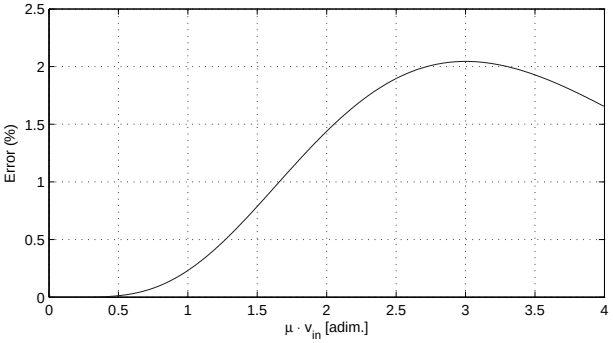

Figure 3: Percentage error introduced by (7) and (8).

of μv_{in} only. However, analytical derivation of the dependence $E(\mu v_{\text{in}})$ have been classically performed in the limit of small initial velocities and/or small dissipation [6].

A non-local approximation for v_{out} can be empirically determined by fitting the curve $E(\mu v_{\text{in}})$ in the two limit regions $\mu v_{\text{in}} \to 0$ and $\mu v_{\text{in}} \to \infty$, giving

$$v_{\text{out}}(\mu, v_{\text{in}}) = v_{\text{lim}}\left[1 - \left(\sum_{j=0}^{n} b_j \cdot v_{\text{in}}^j\right) e^{-2\mu v_{\text{in}}}\right], \tag{7}$$

where, in the case $n = 4$, the coefficients b_j are

$$b_0 = 1, \quad b_1 = \mu, \quad b_2 = \frac{2}{3}\mu^2, \quad b_3 = \frac{2}{9}\mu^3, \quad b_4 = \frac{14}{135}\mu^4. \tag{8}$$

Figure 3 shows the error introduced by (7) for $n = 4$ and the coefficients (8), when compared to the corresponding value computed numerically as a zero of (6).

2.1.3. Contact time

It is shown in [14] that the contact time can be expressed as

$$\tau = \left(\frac{m}{k}\right)^{\frac{1}{\alpha+1}} \cdot \left(\frac{\mu^2}{\alpha+1}\right)^{\frac{\alpha}{\alpha+1}} \cdot \cdot \int_{v_{\text{out}}}^{v_{\text{in}}} \frac{1}{(1+\mu v)\left[-\mu(v-v_{\text{in}}) + \log\left|\frac{1+\mu v}{1+\mu v_{\text{in}}}\right|\right]^{\frac{\alpha}{\alpha+1}}}. \quad (9)$$

Equation (9) states that the contact time τ depends only on μ, the exponent α, and the ratio m/k, plus obviously the impact velocity v_{in}. Since neither m nor k affect the value of the integral (recall that v_{out} depends only on μ and v_{in}), it follows that, given a fixed v_{in}, the power-law dependence $\tau \sim (m/k)^{1/(\alpha+1)}$ holds.

From an auditory point of view, the value of the contact time is strongly correlated to the perceived "hardness" of the impact [14]. Namely, as the contact time decreases, the perceived hardness increases. Recalling the power-law dependence above and (1) it follows that, for a fixed mass m, "hard" and "soft" impacts correspond respectively to high and low force values.

2.1.4. Energy properties and behavior

The energy variation in a mechanical system can be calculated as the work made by the overall force f acting on the system along a certain path $x_1 \rightarrow x_2$:

$$\Delta H = \int_{x_1}^{x_2} f(x)\, dx = \int_{t_1}^{t_2} f(t)v(t)\, dt \quad (10)$$

where H is the total energy content, known as the *Hamiltonian*, and the second integral is obtained by considering that t_1 and t_2 correspond respectively to the instants when the displacements x_1 and x_2 are reached. The Hamiltonian H is the sum of potential and kinetic energies (named V and T, respectively):

$$H(t) = V(t) + T(t). \quad (11)$$

With regard to the system represented by (2), T is related to the dynamics of the point-mass, which is described by the left-hand side of (2), while V is related to the elastic component of the impact force given in (1).

More specifically, and in agreement with the last integral in (10), multiplying both sides of (2) by $v(t) = dx/dt$ and time-integrating them, gives

$$\underbrace{\int ma(t)v(t)\, dt}_{T(t)} = -\underbrace{\int kx(t)^{\alpha}v(t)\, dt}_{V(t)} - \underbrace{\int \lambda x(t)^{\alpha}v(t)^2\, dt}_{\Lambda(t)} \quad (12)$$

where the force expression given in (1) has been considered in the case $x > 0$ only, and $\Lambda(t)$ is the work made by the dissipative component of the impact force. The integrals $V(t)$ and $T(t)$ in (12) can be solved explicitly, giving

$$V(t) = \frac{kx(t)^{\alpha+1}}{\alpha+1}, \quad T(t) = \frac{mv(t)^2}{2}. \quad (13)$$

Now consider a system where the point-mass travels with velocity v_{in} before the impact occurs, then the initial Hamiltonian corresponds to the initial kinetic energy and is

$$H_0 = T_0 = \frac{mv_{\text{in}}^2}{2}. \quad (14)$$

From (12) and (14), and recalling the *principle of conservation of energy*, it follows that at each time instant t:

$$\begin{aligned} & V(t) + T(t) + \Lambda(t) = H_0 \\ \Rightarrow \quad & H(t) = H_0 - \Lambda(t). \end{aligned} \quad (15)$$

Moreover from (15) follows that, at every time instant t, the overall variation of energy is:

$$\Delta H(t) = H(t) - H_0 = -\Lambda(t), \quad (16)$$

and therefore the total amount of energy dissipation occurred during the impact interaction is

$$\Delta H_\tau = H_\tau - H_0 = -\Lambda_\tau, \quad (17)$$

where τ indicates the instant when the impact ends, and H_τ is the final Hamiltonian of the system, that is the energy content after the impact interaction has ended, which equals:

$$H_\tau = T_\tau = \frac{mv_{\text{out}}^2}{2}. \quad (18)$$

It can be noted that ΔH_τ corresponds to the area enclosed by the hysteresis loops represented in figure 2.

As a last remark, from the results above it clearly follows that

$$0 \leq H(t + dt) \leq H(t). \quad (19)$$

3. NUMERICAL SIMULATIONS

In this section, the continuous-time system described by (2) is discretized by means of several numerical methods, and the resulting numerical systems are studied.

3.1. Remarks on accuracy and stability

All numerical systems can simulate their continuous-time counterparts only to some extent. Generally speaking, one of the basic reasons for this inherent limit is that the discretized variables depend on the chosen *sample rate* F_s, and therefore the behavior of any numerical method is bounded by it.

For instance, since our numerical system takes as input the initial velocity v_{in} of the point-mass, the compression x can only be computed as a function (integral) of v_{in}[1]. It is clear that, much as good a numerical method can be, the higher v_{in} and/or the lower F_s (i.e., less samples are available for computing the numerical integral) are, the less precise x is. In any case, the computed compression is *always* an approximate value.

Besides, the resulting impact force f is obviously affected too, and as the impact "hardness" increases, the computation error increases as well. From a more general perspective, those inconsistencies are reflected in the energy behavior of the numerical system: for example, it is evident that inconsistently large compressions cause the force, the output velocity, and therefore the energy, to increase inconsistently with the continuous-time system.

Apart from the intrinsic numerical bounds pointed above, it must be noted that different numerical methods behave differently, and that *all* of them are susceptible to problems related to stability.

[1] It is clear that, while the dependence on the impact velocity has a physical meaning, the dependence on the sample rate has not.

For instance, for some values of parameters, one method could dissipate too much energy, while another one could violate the principle of passivity, thus generating spurious energy. In both cases those inconsistencies - besides the fact of resulting in an erroneous state of the system - could give birth to instabilities.

Even though some stability conditions can be derived for LTI systems[2], those do not extend to the case of non-linear systems. In the latter case one possibility is to exploit energy-based methods (see for example [16] in the context of physical modeling sound synthesis).

3.2. Numerical methods

Hereafter, the continuous-time system of (2) is discretized using different numerical methods. Following the standard notation in numerical mathematics, the integration step is a constant named h.

3.2.1. 1-step Adams-Moulton

The *1-step Adams-Moulton* (AM1) [15] is a A-stable 2nd-order implicit method, also known as *bilinear transformation*, or *trapezoidal rule*.

Discretizing the equation of motion (left-hand side of (2)) results in the following state-space form equation:

$$\begin{bmatrix} x_{n+1} \\ v_{n+1} \end{bmatrix} = \begin{bmatrix} 1 & h \\ 0 & 1 \end{bmatrix} \begin{bmatrix} x_n \\ v_n \end{bmatrix} + \begin{bmatrix} \frac{h^2}{4m} \\ \frac{h}{2m} \end{bmatrix} [f_{n+1} + f_n]. \quad (20)$$

where the expression for the discrete-time force can be obtained by replacing the continuous-time variables $x(t)$ and $v(t)$ in (1) with their discrete-time counterparts.

Since the AM1 method is implicit, (20) is also in implicit form and this is reflected in the instantaneous relationship between $[x_{n+1}\ v_{n+1}]^T$ and f_{n+1}. Unfortunately, since f_{n+1} also has an instantaneous dependence on x_{n+1} and v_{n+1}, the discrete-time counterpart of the system described by (2) contains a delay-free loop, which is not directly computable and – because of the included non-linearities – needs some special handling in order to be solved. In particular, the *K-method* [17] together with *Newton's method* [15] are used, weighing on the efficiency of the simulation.

3.2.2. Velocity Verlet

The *Verlet method* [18] is a 2nd-order explicit method which is commonly used in computer graphics [1], video games, and molecular dynamics simulation. Its main application is that of integrating Newton's equation of motion in order to describe the trajectory of moving particles. The one used here is a variant called *velocity Verlet*, which provides better handling of the velocity variable and can be seen as a predictor-corrector method.

Discretizing the system represented in (2), results in the following implementation scheme:

$$\begin{aligned} x_{n+1} &= x_n + h v_n + \frac{h^2}{2}\frac{f_n}{m} \\ v_{n+\frac{1}{2}} &= v_n + \frac{h}{2}\frac{f_n}{m}, \quad \text{predictor} \\ f_{n+1} &= f(x_{n+1}, v_{n+\frac{1}{2}}), \\ v_{n+1} &= v_{n+\frac{1}{2}} + \frac{h}{2}\frac{f_{n+1}}{m}, \quad \text{corrector.} \end{aligned} \quad (21)$$

[2] Consider, for example, the von Neumann analysis [15].

It should be noted that this algorithm assumes that f_{n+1} only depends on the predicted velocity $v_{n+\frac{1}{2}}$, which clearly gives rise to inaccuracies.

3.2.3. Heun

The *Heun method* [15] is a predictor-corrector explicit method, with the forward Euler method as predictor and the trapezoidal rule as corrector. It can also be seen as a *2nd-order Runge-Kutta method* (RK2).

Discretizing (2) results in the following implementation scheme:

$$\begin{aligned} \tilde{v}_{n+1} &= v_n + h\frac{f_n}{m}, \quad \text{predictor} \\ x_{n+1} &= x_n + \frac{h}{2}(v_n + \tilde{v}_{n+1}) \\ f_{n+1} &= f\left(x_{n+1}, \tilde{v}_{n+1}\right), \\ v_{n+1} &= v_n + \frac{h}{2}\frac{f_n + f_{n+1}}{m}, \quad \text{corrector.} \end{aligned} \quad (22)$$

Again, it should be noted that both x_{n+1} and f_{n+1} only depend on the predicted velocity $\tilde{v}_{n+1}$, and this gives rise to inaccuracies.

3.2.4. 4th-order Runge-Kutta

The *4th-order Runge-Kutta* [15] is an explicit iterative method which is widely used to solve ODEs with improved accuracy.

Discretizing (2) results in the following implementation scheme:

$$\begin{aligned} x_{n+1} &= x_n + \frac{1}{6}(l_1 + 2l_2 + 2l_3 + l_4) \\ v_{n+1} &= v_n + \frac{1}{6}(k_1 + 2k_2 + 2k_3 + k_4) \end{aligned} \quad (23a)$$

where

$$\begin{aligned} l_1 &= h v_n, \quad l_2 = h(v_n + \frac{k_1}{2}), \\ l_3 &= h(v_n + \frac{k_2}{2}), \quad l_4 = h(v_n + k_3) \\ k_1 &= h\frac{f_n}{m}, \quad k_2 = h\frac{f(x_n + \frac{l_1}{2}, v_n + \frac{k_1}{2})}{m}, \\ k_3 &= h\frac{f(x_n + \frac{l_2}{2}, v_n + \frac{k_2}{2})}{m}, \quad k_4 = h\frac{f(x_n + l_3, v_n + k_3)}{m}. \end{aligned} \quad (23b)$$

It should be noted that, for each sample, both the velocity and the non-linear force given in (1) need to be evaluated four times, therefore affecting the efficiency of the simulation.

3.3. Experimental results

In order to evaluate the chosen numerical methods, it is useful to compare the behavior of the corresponding simulations against the known analytical results (cfr. section 2.1).

In particular, several plots are provided which show: the phase portrait on the (x, v) plane (cfr. figure 1), the compression-force characteristic (cfr. figure 2) and, in the discrete-time domain, the impact force f and the Hamiltonian H.

The following values of parameters are kept constant throughout the simulations: $m = 10^{-2}$ kg, and $F_s = 44.1$ kHz, that is a standard audio sample rate. The considered integration step h is therefore equal to $1/F_s$.

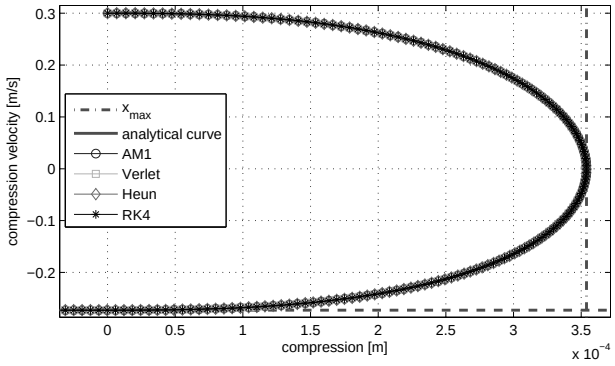

(a) Phase portraits.

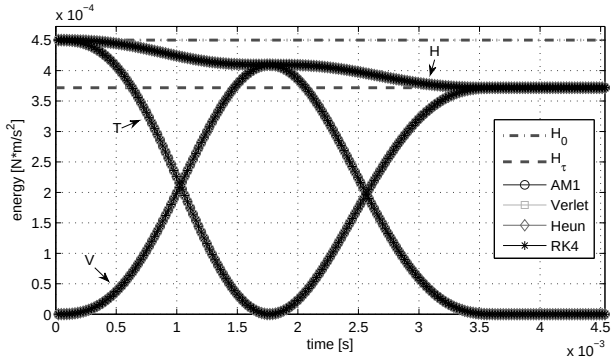

(b) Energy behaviors.

Figure 4: Comparison of different methods in a soft impact case. The values of parameters are $k = 10^6$ N/m$^\alpha$, $\mu = 0.5$ s/m, $\alpha = 1.6$, $v_{\text{in}} = 0.3$ m/s.

3.3.1. *Reference simulations: Soft impact*

In order to verify the simulations and provide a reference, the model's parameters are set to a "soft" configuration where the impact interaction extends over many samples, so that the numerical systems operate in a safe space and should therefore behave very similarly to the original continuous-time system.

This is confirmed by figure 4, where the plots of all the simulations substantially overlap. In particular, it is possible to check the accuracy of the simulations against the analytical results provided in section 2.1: figure 4(a) displays the phase portrait on the (x, v) plane and, as tangent lines, the maximum compression x_{max} and the output velocity v_{out}, while in figure 4(b) two horizontal lines display $H_0 = T_0$ and $H_\tau = T_\tau$, that is respectively the initial and the final Hamiltonian.

Figure 4(b) also allows to understand the energy behavior of the system: the sinusoid-like curves represent the kinetic energy T (curve starting at $H_0 = T_0$) and the elastic potential energy V (curve starting at 0). The sum of the potential and kinetic energies provides the upper staircase-like curve representing the Hamiltonian H, which indeed decreases[3] until $H_\tau = T_\tau$ in correspondence to the end of the contact interaction.

[3]When $\mu = 0$ the overall energy remains constant, that is $H = H_0 = H_\tau$.

3.3.2. *General study*

It can be observed that for hard impacts (that is when the contact time lasts only a few samples) and/or when $\mu v_{\text{in}} \to 0_+$, the energy behavior of some numerical implementations becomes inconsistent with the continuous-time system.

The main reference used to qualitatively and/or quantitatively assess the reliability of a particular numerical method is the energy behavior of the corresponding simulation. In particular, the following condition

$$H_{n+1} \leq H_n, \quad \text{for all } n \tag{24}$$

should be satisfied (see (19)). Other indicators are provided by the analytical values of maximum compression x_{max} and output velocity v_{out}, which should never be exceeded.

It is found empirically that when $\tau \leq 4$ samples, the percentage errors quickly increase, and the reliability of all the simulations is poor. Hence, for the sake of clarity, in the study hereafter only values of parameters resulting in $\tau > 4$ samples are considered.

Case 1: $\mu v_{\text{in}} \to 0_+$

Even in case of "not-too-hard" impacts[4], the Hamiltonian of both Verlet- and Heun-discretized systems is prone to oscillations, and the system generally results in an inconsistent final energy state (typically, $H_\tau^{\text{Verlet, Heun}} > H_\tau$). Moreover, as put forward in section 3.1, for hard impacts (high k and/or low α) the maximum compression is often higher than the analytical value x_{max}. As for AM1-discretized systems, these generally tend to dissipate too much energy during the compression phase, while gaining spurious energy during the decompression phase (i.e. $H_\tau^{\text{AM1}} > H_\tau$). On the other hand, RK4-discretized systems generally behave quite consistently (i.e. $H_\tau^{\text{RK4}} \approx H_\tau$).

Figure 5 shows an example simulation of hard impact (contact time = 8 samples) with $\mu v_{\text{in}} = 0.03$, while table 1(a) shows the corresponding percentage errors.

Case 2: hard impacts with average or high values of μv_{in}

During the impact interaction, all the simulations usually result in a sufficiently consistent time evolution of the Hamiltonian: the condition (24) is generally satisfied, except for the end of the interaction.

At this stage, the two 2nd-order explicit methods typically tend to introduce spurious energy (i.e. $H_\tau^{\text{Verlet, Heun}} > H_\tau$). Concerning AM1-discretized systems, these tend to behave better than the two methods mentioned above, even if sometimes $H_\tau^{\text{AM1}} > H_\tau$. Again, RK4-discretized systems generally behave rather consistently, and only experience small discrepancies from the analytical results (i.e. $x_{\text{max}}^{\text{RK4}} \approx x_{\text{max}}$ and $H_\tau^{\text{RK4}} \approx H_\tau$).

A second hard impact example simulation is provided, following the values of parameters adopted in figure 1 for $v_{in} = 1$ m/s ($\mu v_{\text{in}} = 0.5$), while table 1(b) shows the corresponding percentage errors. The resulting contact time τ equals 6 samples.

From the simulations above it is clear that the percentage error is not strictly correlated to the impact hardness (that is, the duration in samples of the contact interaction). Moreover, the nonlinearities of the impact model described by (1) make it difficult to predict the exact behavior of the corresponding numerical system, especially with lower-order explicit methods.

[4]e.g., when the contact time lasts tens of samples

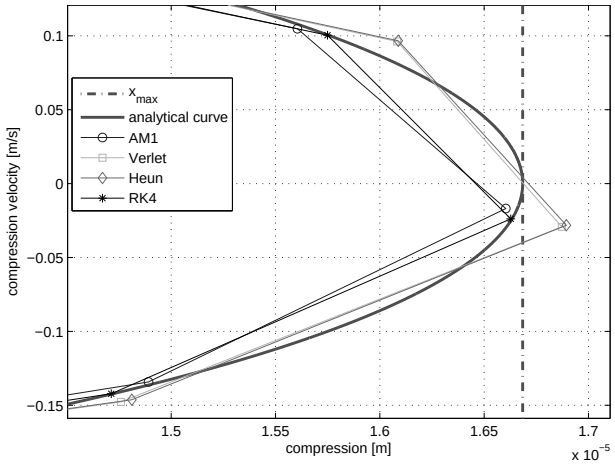

(a) Detail of phase portraits.

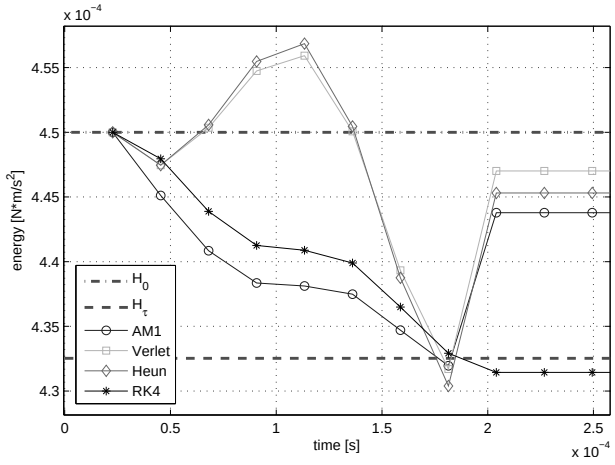

(b) Detail of energy behaviors.

Figure 5: Hard impact example following *case 1*: Comparison of different numerical methods. The values of parameters are $k = 10^7$ N/m$^\alpha$, $\mu = 0.1$ s/m, $\alpha = 1.1$, $v_{\text{in}} = 0.3$ m/s. The contact time equals 8 samples.

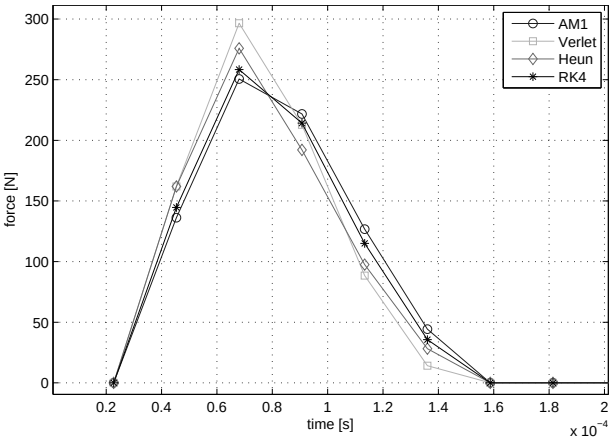

(a) Impact forces.

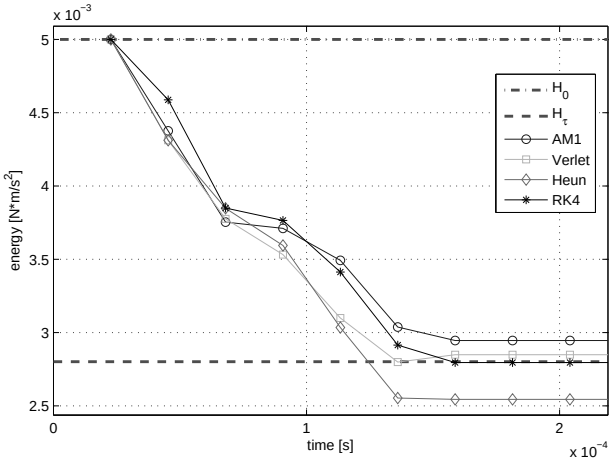

(b) Detail of energy behaviors.

Figure 6: Hard impact example following *case 2*: Comparison of different numerical methods. The values of parameters are the same as in figure 1 with $v_{\text{in}} = 1$ m/s. The contact time equals 6 samples.

4. IMPROVED NUMERICAL SIMULATIONS

4.1. Contact sound models

Contact models borrowed from different application fields can serve as a basis for developing models of acoustic phenomena. As an example, in the context of physical sound modeling, the impact model described by (2) has already been used to develop an impact sound model [3], namely by substituting the rigid wall component with a generic resonating object. Also, other models of more complex sound phenomena have been based on the very same impact model studied here. As a basic example, a *bouncing* sound model [19] has been obtained by superimposing a constant force, which simulates gravity, on a plain impact sound model. Moreover, a *rolling* sound model [20] has been developed by driving an impact sound model by means of a sophisticated control layer. More precisely, the continuous interaction of a ball rolling on a surface has been modeled as a dense temporal sequence of micro-impacts driven by the geometry of the contacting surfaces and modulated by the ball's asymmetry.

From these application examples it is clear that, even if the errors are generally tolerably small[5] for single impact events, in case of sustained contacts or multiple impacts the energy state of the system can become strongly inconsistent. This is a known issue also in computer graphics, where the constraint of low frame rates makes numerical systems prone to instabilities [1]. An example is that of a steady object in sustained contact with a rigid floor: when the system does not retain passivity, the object can move upward and bounce. Similar issues are encountered in simulation of haptic contact, where stiffness values are usually limited by requirements on system passivity [21], whereas higher values can cause the system to become unstable, i.e., to oscillate uncontrollably.

[5] Especially if $\tau > 4$ samples, and when using implicit or high-order numerical methods.

(a) Simulation example following *case 1*. The values of parameters are the same as in figure 5.

%err	AM1	Verlet	Heun	RK4	num. res.
$x_{\max}$	n.e.	$+1.122$	$+1.254$	n.e.	-
v_{out}	$+1.293$	$+1.660$	$+1.467$	-0.125	$\sim -10^{-2}$
H_{tau}	$+2.603$	$+3.348$	$+2.955$	-0.250	-

(b) Simulation example following *case 2*. The values of parameters are the same as in figure 1 for $v_{\text{in}} = 1$ m/s.

%err	AM1	Verlet	Heun	RK4	num. res.
$x_{\max}$	n.e.	n.e.	n.e.	n.e.	-
v_{out}	$+2.551$	$+0.839$	-4.692	-0.105	$\sim -10^{-4}$
H_{tau}	$+5.166$	$+1.685$	-9.164	-0.211	-

Table 1: Summary of percentage errors for two hard-impact example simulations. The caption "n.e." stands for "not exceeded". The last column shows the error resulting from comparing the approximate value v_{out}, which is obtained from (7) and (8), against a value computed numerically as a zero of (6) (cfr. figure 3).

4.2. Exploitation of analytical results

In this section, some solutions are proposed to partially fix the inconsistencies pointed out in section 3.3. The aim is to improve the reliability of simulations which use the impact model under study, in view of their implementation as real-time applications.

As written above, in order for the numerical systems to behave consistently, the energy condition given in (24) must hold. Moreover, from figure 1 it can be inferred that the relation $v(t+dt) \leq v(t)$ holds. This brings us to the following condition:

$$v_{n+1} \leq v_n, \quad \text{for all } n. \tag{25}$$

However, at the time of writing no analytical result describing the behavior of the state variables $x(t)$ and $v(t)$ over time is available, and therefore there is no easy option that allows to fix wrong numerical values of H or v *during* the impact interaction.

One indirect approach is to intervene on the compression, for which the following condition must hold:

$$x_n \leq x_{\max}, \quad \text{for all } n, \tag{26}$$

where $x_{\max}$ is a constant calculated by (4). Hence the suggested solution is that of clipping x_n to the maximum allowable value $x_{\max}$ whenever this is exceeded. This also affects the Hamiltonian of the system by decreasing the elastic potential energy V_n.

An additional solution is to force the numerical output velocity to the approximate value v_{out} calculated by (7) and (8). As a result, as the interaction ends the energy content of the numerical system is restored, that is the Hamiltonian is forced to H_τ. Since the error introduced by the approximate value of v_{out} – even in case of hard impacts – is generally of order lower than that of the error introduced by the numerical simulations (cfr. table 1), the correction of v_{out} ensures that the physical consistency of the numerical system is improved.

In order to implement the suggested corrections, it is necessary to compute the values of $x_{\max}$ and v_{out}, which are given respectively by (4), and (7) plus a nth-order expansion for the coefficients b_j (e.g., the 4th-order expansion (8)). These computations only need to take place in correspondence of an impact event, and more precisely as soon as the impact velocity v_{in} is known.

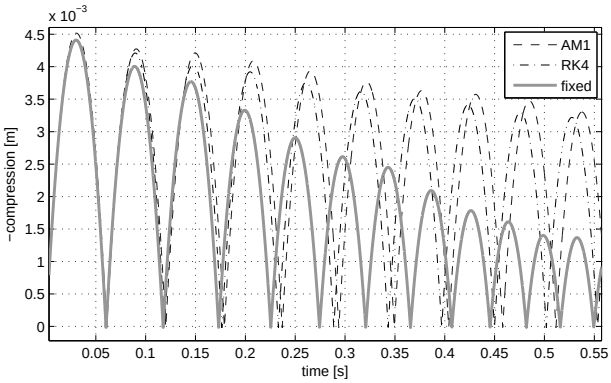

Figure 8: Effect of errors when the force of gravity is applied to the simulation example of *case 1*. For the sake of clarity, the sign of the compression has been inverted, this way visually representing the rebounds as they would occur on a horizontal floor.

4.3. Numerical simulations with corrections

As a basic application example, the worst behaving impact simulations found in *case 1* and in *case 2* of section 3.3.2 were corrected using the solutions explained above. Figure 7 shows a comparison of the simulations with and without corrections. In the corrected simulations, the compression is limited to $x_{\max}$ and the energy content is forced to H_τ upon the end of the interaction.

Furthermore, in order to verify the necessity of corrections even in case of small errors, an external force was applied to the point-mass, this way simulating a bouncing object. It is found that when the point-mass travels with even slightly wrong velocities, the trajectories are inaccurate, the rebounds happen at the wrong time, energy is wrongly dissipated, and above all those errors accumulate at each impact event. Figure 8 shows the effect of small errors in the situation pointed above, where the force of gravity $f_g = mg$ is superimposed on the impact simulation example provided in section 3.3.2 and corresponding to *case 1*. Note that, in order to stress that even small errors can strongly affect the physical consistency, only the two *best* performing simulations (namely, AM1 and RK4) are portrayed.

5. CONCLUSIONS

A non-linear physical model of impact with sound synthesis applications has been reviewed, and its properties have been studied using both analytical tools and numerical simulations.

Several numerical realizations have been compared, and their shortcomings with regard to the corresponding analytical results have been shown. Special emphasis has been placed on energy consistency.

Moreover, it has been shown that by exploiting some analytical results, the inconsistencies of the numerical realizations can be amended, thus restoring the correct energy state of the simulated systems after the impact interaction has ended. On the other hand, an efficient way to control the energy content of the system throughout the contact interaction is still needed.

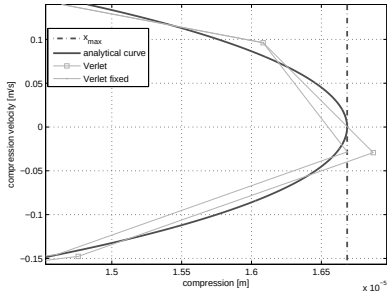

(a) *Case 1*: phase portrait of the Verlet-discretized system. The compression x is forced to $x_{\max}$.

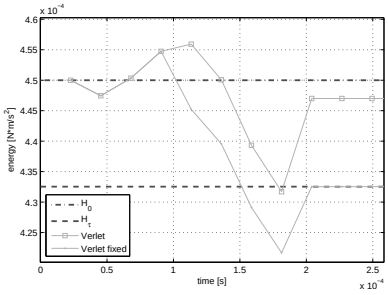

(b) *Case 1*: energy behavior of the Verlet-discretized system. During the interaction, the Hamiltonian is influenced by the correction of x, and as the interaction ends, the velocity is forced to v_{out}, resulting in $H = H_\tau$.

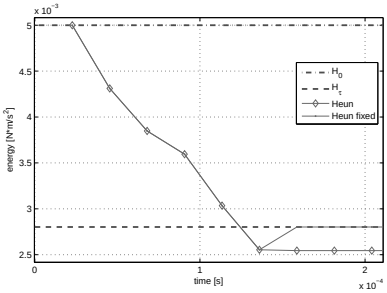

(c) *Case 2*: energy behavior of the Heun-discretized system. As the interaction ends, the velocity is forced to v_{out}, resulting in $H = H_\tau$.

Figure 7: Comparison of simulations with and without corrections.

6. ACKNOWLEDGMENTS

The research leading to these results has received funding from the EU's Seventh Framework Programme under FET-Open grant agreement n°222107 NIW - Natural Interactive Walking.

7. REFERENCES

[1] M. Müller, J. Stam, D. James, and N. Thürey, "Real time physics: class notes," in *SIGGRAPH '08: ACM SIGGRAPH 2008 classes*, New York, NY, USA, 2008, pp. 1–90, ACM.

[2] A. Chaigne and J. Kergomard, *Acoustique des Instruments de Musique*, Belin, 2008.

[3] F. Avanzini and D. Rocchesso, "Modeling collision sounds: non-linear contact force," in *Proc. Int. Conf. on Digital Audio Effects (DAFx-01)*, Limerick, December 2001, pp. 61–66.

[4] P. Flores, J.C. Pimenta Claro, and H. M. Lankarani, *Kinematics and Dynamics of Multibody Systems with Imperfect Joints: Models and Case Studies*, Springer, 2008.

[5] G. Kuwabara and K. Kono, "Restitution coefficient in a collision between two spheres," *Jap. J. of Appl. Phys.*, vol. 26, no. 8, pp. 1230–1233, 1987.

[6] K. H. Hunt and F. R. E. Crossley, "Coefficient of restitution interpreted as damping in vibroimpact," *ASME J. Applied Mech.*, pp. 440–445, June 1975.

[7] D. W. Marhefka and D. E. Orin, "A compliant contact model with nonlinear damping for simulation of robotic systems," *IEEE trans. on Systems, Man, and Cybernetics - Part A: Systems and Humans*, vol. 29, no. 6, pp. 566–572, November 1999.

[8] N. Diolaiti, C. Melchiorri, and S. Stramigioli, "Contact impedance estimation for robotic systems," *IEEE Transactions on Robotics*, vol. 21, no. 5, pp. 925–935, 2005.

[9] H. M. Lankarani and P. E. Nikravesh, "A contact force model with hysteresis damping for impact analysis of multibody systems," *Journal of Mechanical Design*, vol. 112, no. 3, pp. 369–376, 1990.

[10] P. Flores, J. Ambrósio, J. Claro, and H. Lankarani, "Influence of the contact-impact force model on the dynamic response of multi-body systems," *Proceedings of the Institution of Mechanical Engineers-K*, vol. 220, no. 1, pp. 21–34, 2006.

[11] L. Pust and F. Peterka, "Impact oscillator with Hertz's model of contact," *Meccanica*, vol. 38, no. 1, pp. 99–116, 2003.

[12] A. Stulov, "Dynamic behavior and mechanical features of wool felt," *Acta Mechanica*, vol. 169, no. 1, pp. 13–21, 2004.

[13] L. Vu-Quoc and X. Zhang, "An elastoplastic contact force-displacement model in the normal direction: displacement-driven version," *Proceedings: Mathematical, Physical and Engineering Sciences*, pp. 4013–4044, 1999.

[14] F. Avanzini and D. Rocchesso, "Physical modeling of impacts: theory and experiments on contact time and spectral centroid," in *Proc. Int. Conf. on Sound and Music Computing (SMC'04)*, 2004, pp. 287–293.

[15] A. Quarteroni, R. Sacco, and F. Saleri, *Numerical Mathematics*, Springer, 2nd edition, 2007.

[16] S. Bilbao, "Robust physical modeling sound synthesis for nonlinear systems," *Signal Processing Magazine, IEEE*, vol. 24, no. 2, pp. 32–41, March 2007.

[17] G. Borin, G. De Poli, and D. Rocchesso, "Elimination of Delay-Free Loops in Discrete-Time Models of Nonlinear Acoustic Systems," *IEEE Trans. on Speech and Audio Processing*, vol. 8, no. 5, pp. 597–605, September 2000.

[18] L. Verlet, "Computer "Experiments" on Classical Fluids. I. Thermodynamical Properties of Lennard-Jones Molecules," *Physical Review*, vol. 159, no. 1, pp. 98+, July 1967.

[19] D. Rocchesso and F. Fontana, Eds., *The Sounding Object*, Mondo Estremo, 2003, Available at http://www.soundobject.org/.

[20] M. Rath and D. Rocchesso, "Continuous sonic feedback from a rolling ball," *IEEE MultiMedia*, vol. 12, no. 2, pp. 60–69, 2005.

[21] J. Edward Colgate and J. Michael Brown, "Factors Affecting the Z-Width of a Haptic Display," in *Proc. IEEE Int. Conf. on Robotics & Automation*, San Diego, May 1994, pp. 3205–3210.